Accurate Tracking of Aggressive Quadrotor Trajectories using Incremental Nonlinear Dynamic Inversion and Differential Flatness

Ezra Tal Sertac Karaman

***Abstract*— In this paper, we propose a novel control law for accurate tracking of aggressive (*i.e.*, high-speed and high-acceleration) quadcopter trajectories. The proposed method tracks position and yaw angle with their derivatives of up to fourth order, specifically, the position, velocity, acceleration, jerk, and snap along with the yaw angle, yaw rate and yaw acceleration. Two key aspects of the proposed method are the following. First, the controller exploits the *differential flatness* of the quadcopter dynamics to generate feedforward inputs for attitude rate and attitude acceleration in order to track the jerk and snap references. The tracking is enabled by direct control of body torque using closed-loop control of all four propeller speeds based on optical encoders attached to the motors. Second, the controller utilizes the *incremental nonlinear dynamic inversion (INDI)* method for accurate tracking of linear and angular accelerations despite external disturbances. Hence, no prior modeling of aerodynamic effects is required. We evaluate the proposed control law in experiments under motion capture. Using a 1-kg quadcopter, we are able to track a complex 3D trajectory, reaching speeds up to 8.2 m/s and accelerations up to 2g, while keeping the root-mean-square tracking error down to 4.0 cm, in a flight volume that is roughly 6.5 m long, 6.5 m wide, and 1.5 m tall.**

Supplemental Material

A video of the experiments can be found at `https://youtu.be/M1lE9MlFmVA`. An extended version of this paper, including the derivation of the controller, a rigorous analysis, and more extensive experimental results, is available [1].

I. Introduction

Accurate control of the aircraft during aggressive, *i.e.*, high-speed and high-acceleration maneuvers is essential towards enabling fully-autonomous drone flight. At high speeds, the aerodynamic drag — which is hard to model — becomes a dominant factor. Accounting for aerodynamics is an important challenge in control design for vehicles operating at high speeds. Recent research has addressed this challenge through modeling [2]–[4], estimation [5], [6], and learning [7] of such aerodynamic drag effects towards tracking of high-speed trajectories.

In this paper, we propose a control system for accurate trajectory tracking during aggressive maneuvering of quadcopter aircraft, such as the one shown in Figure 1. The controller exploits the differential flatness of the quadcopter dynamics to generate feedforward control terms based on the reference trajectory and its derivatives up to fourth order, *i.e.*, position, velocity, acceleration, jerk, and snap along with yaw angle, yaw rate, and yaw acceleration. Incremental nonlinear dynamic inversion (INDI) is relied upon to handle external disturbances, *e.g.*, aerodynamic drag forces, without the need for modeling or estimation of drag parameters.

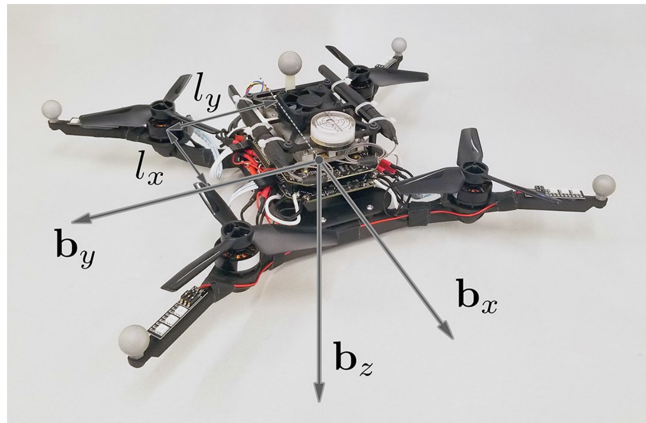

Fig. 1: Quadrotor with body-fixed reference system and moment arm definitions.

The INDI technique has recently been developed [8], [9], based on earlier derivations [10], [11], which provide robustness by incrementally applying control inputs based on inertial measurements. As such, it is able to alleviate robustness issues from which regular nonlinear dynamic inversion (NDI) controllers commonly suffer. INDI has been applied to quadcopters for stabilization, *e.g.*, for robust hovering [12], [13], but not for trajectory tracking.

The differential flatness property allows expressing all states and inputs of a dynamic system in terms of a set of flat outputs and its derivatives [14]. In the context of flight control, this property enables reformulation of the trajectory tracking problem as a state tracking problem [15], [16], which has also been applied to quadcopter trajectory tracking [2], [17]–[19].

The control design presented in this paper is novel in the following ways. Firstly, we develop a new control methodology that enables the tracking of snap by accurately controlling motor speeds. We recognize that snap is directly related to vehicle angular accelerations, which can be tracked by direct application of body torque commands. We achieve such application of body torques through closed-loop control of the motor speeds using measurements from optical encoders attached to each motor. To the best of our knowledge, the direct control over snap using motor speed measurements is novel. In contrast, trajectory tracking control based on body rate inputs — *e.g.*, using a typical inner-loop flight

E. Tal and S. Karaman are with the Department of Aeronautics and Astronautics and the Laboratory for Information and Decision Systems, Massachusetts Institute of Technology (MIT), Cambridge, MA 02139, USA. `{eatal,sertac}@mit.edu`

controller — is incapable of truly considering reference snap. Secondly, we develop a novel INDI control design for quadcopter trajectory tracking. To the best of the our knowledge, the proposed controller is the first design that is tailored for trajectory tracking, as existing INDI control designs focus on state regulation, *e.g.*, for maintaining hover under external disturbances. Finally, we demonstrate the proposed controller in experiments, in which the proposed control law enables a 1-kg quadcopter to track complex 3D trajectories, reaching speeds up to 8.2 m/s and accelerations up to 2g, while keeping the root-mean-square tracking error down to 4 cm, in a flight volume that is roughly 6.5 m long, 6.5 m wide, and 1.5 m tall.

The paper is structured as follows: In Section II, the quadrotor model is specified, and we show how feedforward control inputs are formulated in terms of the reference trajectory using differential flatness. In Section III, we describe the architecture of the trajectory tracking controller. Finally, we give experimental results from real-life flights in Section IV.

II. Preliminaries

In this section, we describe the quadrotor dynamics and we show how the differential flatness property is utilized to derive feedforward attitude rate and attitude acceleration references. For full the derivation of the differential flatness results, the reader is referred to [1].

A. Quadrotor Model

We consider a 6 degree-of-freedom (DOF) quadrotor, as shown in Fig. 1. The depicted basis vectors of the body-fixed reference frame form the rotation matrix $\mathbf{R} = [\mathbf{b}_x\ \mathbf{b}_y\ \mathbf{b}_z] \in SO(3)$, which gives the transformation from the body-fixed reference frame to the inertial reference frame. The columns of the identity matrix $\mathbf{I} = [\mathbf{i}_x\ \mathbf{i}_y\ \mathbf{i}_z]$ give the basis of the inertial reference frame.

The vehicle dynamics are given by

$$\dot{\mathbf{x}} = \mathbf{v}, \tag{1}$$

$$\dot{\mathbf{v}} = g\mathbf{i}_z + \tau\mathbf{b}_z + m^{-1}\mathbf{f}_{ext}, \tag{2}$$

$$\dot{\boldsymbol{\xi}} = \mathbf{S}\boldsymbol{\Omega}, \tag{3}$$

$$\dot{\boldsymbol{\Omega}} = \mathbf{J}^{-1}(\boldsymbol{\mu} + \boldsymbol{\mu}_{ext} - \boldsymbol{\Omega} \times \mathbf{J}\boldsymbol{\Omega}), \tag{4}$$

where $\mathbf{x}$ and $\mathbf{v}$ are the position and velocity in the inertial reference frame, respectively, $\boldsymbol{\xi} = [\phi\ \theta\ \psi]^T$ is the roll-pitch-yaw Euler attitude vector, and $\boldsymbol{\Omega} = [p\ q\ r]^T$ is the angular velocity in the body-fixed reference frame. The gravitational acceleration is indicated by g, the specific trust, *i.e.*, the ratio of total thrust T and the vehicle mass m, by τ, and the control moment vector by $\boldsymbol{\mu}$. The matrices $\mathbf{J}$ and $\mathbf{S}$ are respectively the vehicle moment of inertia tensor, and the transformation matrix relating attitude rate $\dot{\boldsymbol{\xi}}$ and angular velocity $\boldsymbol{\Omega}$. Finally, the external disturbance force $\mathbf{f}_{ext}$ and moment $\boldsymbol{\mu}_{ext}$ account for all remaining forces and moments acting on the vehicle, including, *e.g.*, aerodynamic drag.

The total thrust T and control moment $\boldsymbol{\mu}$ are a function of the four-element vector of rotor speeds $\boldsymbol{\omega}$, according to

$$\begin{bmatrix} \boldsymbol{\mu} \\ T \end{bmatrix} = \mathbf{G}_1\boldsymbol{\omega}^{\circ 2} + \mathbf{G}_2\dot{\boldsymbol{\omega}}, \tag{5}$$

where $\circ$ indicates the Hadamard power,

$$\mathbf{G}_1 = \begin{bmatrix} l_y k_\tau & -l_y k_\tau & -l_y k_\tau & l_y k_\tau \\ l_x k_\tau & l_x k_\tau & -l_x k_\tau & -l_x k_\tau \\ -k_{\mu_z} & k_{\mu_z} & -k_{\mu_z} & k_{\mu_z} \\ -k_\tau & -k_\tau & -k_\tau & -k_\tau \end{bmatrix}, \tag{6}$$

with l_x and l_y the moment arms indicated in Fig. 1, k_τ and k_{μ_z} indicate the motor thrust and torque coefficients, respectively, and

$$\mathbf{G}_2 = \begin{bmatrix} 0 & 0 & 0 & 0 \\ 0 & 0 & 0 & 0 \\ -J_{r_z} & J_{r_z} & -J_{r_z} & J_{r_z} \\ 0 & 0 & 0 & 0 \end{bmatrix} \tag{7}$$

with J_{r_z} the rotor and propeller moment of inertia. We only consider the z-component of the rotor speed, and note that additional gyroscopic contributions may be neglected [12].

B. Differential Flatness

The differential flatness property enables us to express reference states as a function of the four flat outputs (and their derivatives) given by the reference trajectory function [20]:

$$\boldsymbol{\sigma}_{ref}(t) = [\mathbf{x}_{ref}(t)^T\ \psi_{ref}(t)]^T, \tag{8}$$

which consists of the quadrotor position in the inertial reference frame $\mathbf{x}_{ref}(t) \in \mathbb{R}^3$, and the vehicle yaw angle $\psi_{ref}(t) \in \mathbb{T}$, where $\mathbb{T}$ denotes the circle group. For convenience, we do not explicitly write the time argument t everywhere. We assume that $\mathbf{x}_{ref}$ is of differentiability class C^4, *i.e.*, its first four derivatives exist and are continuous, and that ψ_{ref} is of class C^2. By successive differentiation of $\mathbf{x}_{ref}$, we obtain the reference velocity $\mathbf{v}_{ref}$, the reference acceleration $\mathbf{a}_{ref}$, the reference jerk $\mathbf{j}_{ref}$, and the reference snap $\mathbf{s}_{ref}$. Similarly, we obtain references for the yaw rate $\dot{\psi}_{ref}$, and the yaw acceleration $\ddot{\psi}_{ref}$ by differentiation of ψ_{ref}.

We denote reference states — directly obtained from the reference trajectory — with the same subscript, *i.e.*, ref. The reference states for angular rate and angular acceleration will be applied as feedforward inputs in the trajectory tracking control design.

By taking the derivative of (2), we obtain the following expression for the jerk:

$$\mathbf{j} = \tau\mathbf{R}\,[\mathbf{i}_z]_\times^T\,\mathbf{S}^{-1}\dot{\boldsymbol{\xi}} + \dot{\tau}\mathbf{b}_z, \tag{9}$$

where $[\bullet]_\times$ indicates the cross-product matrix. Equation (9) shows that the jerk is affine in $\dot{\boldsymbol{\xi}}$. Thus, the relation can be inverted to obtain the expression

$$\dot{\boldsymbol{\xi}}_{ref} = \frac{1}{\tau}\begin{bmatrix} -\mathbf{b}_y^T \\ \mathbf{b}_x^T/\cos\phi \\ 0 \end{bmatrix}\mathbf{j}_{ref} + \dot{\psi}_{ref}\begin{bmatrix} \sin\theta \\ -\cos\theta\tan\phi \\ 1 \end{bmatrix}, \tag{10}$$

which gives the reference attitude rate $\dot{\boldsymbol{\xi}}_{ref}$ as a function of $\mathbf{j}_{ref}$ and $\dot{\psi}_{ref}$. We note that $\mathbf{f}_{ext}$ is considered constant here, as its dynamics are unmodeled.

To obtain the attitude accelerations $\ddot{\phi}_{ref}$ and $\ddot{\theta}_{ref}$, we first compute the derivative of (9):

$$\mathbf{s} = \mathbf{R}\left(\ddot{\tau}\mathbf{i}_z + (2\dot{\tau} + \tau[\boldsymbol{\Omega}]_\times)[\mathbf{i}_z]_\times^T \boldsymbol{\Omega} + \tau [\mathbf{i}_z]_\times^T \dot{\boldsymbol{\Omega}}\right), \quad (11)$$

where (by taking the derivative of (3))

$$\dot{\boldsymbol{\Omega}} = -\mathbf{S}^{-1}\dot{\mathbf{S}}\boldsymbol{\Omega} + \mathbf{S}^{-1}\ddot{\boldsymbol{\xi}}. \quad (12)$$

Hence, (11) is affine in $\ddot{\boldsymbol{\xi}}$, and by inversion we obtain the following expression for the reference attitude acceleration $\ddot{\boldsymbol{\xi}}_{ref}$ in terms of $\mathbf{s}_{ref}$ and $\ddot{\psi}_{ref}$:

$$\ddot{\boldsymbol{\xi}}_{ref} = \frac{1}{\tau}\begin{bmatrix} -\mathbf{b}_y^T \\ \mathbf{b}_x^T/\cos\phi \\ 0 \end{bmatrix}\mathbf{s}_{ref} + \ddot{\psi}_{ref}\begin{bmatrix} \sin\theta \\ -\cos\theta\tan\phi \\ 1 \end{bmatrix} - \begin{bmatrix} 1 & 0 & 0 \\ 0 & 1 & 0 \\ 0 & 0 & 0 \end{bmatrix}\mathbf{C}^{-1}\mathbf{e} \quad (13)$$

with

$$\mathbf{C} = \begin{bmatrix} \tau(\mathrm{c}\phi\mathrm{s}\psi - \mathrm{c}\psi\mathrm{s}\phi\mathrm{s}\theta) & \tau\mathrm{c}\phi\mathrm{c}\psi\mathrm{c}\theta & \mathrm{s}\psi\mathrm{s}\phi + \mathrm{c}\psi\mathrm{s}\theta\mathrm{c}\phi \\ -\tau(\mathrm{c}\phi\mathrm{c}\psi + \mathrm{s}\phi\mathrm{s}\psi\mathrm{s}\theta) & \tau\mathrm{c}\phi\mathrm{c}\theta\mathrm{s}\psi & -\mathrm{c}\psi\mathrm{s}\phi + \mathrm{s}\psi\mathrm{s}\theta\mathrm{c}\phi \\ -\tau\mathrm{c}\theta\mathrm{s}\phi & -\tau\mathrm{c}\phi\mathrm{s}\theta & \mathrm{c}\theta\mathrm{c}\phi \end{bmatrix} \quad (14)$$

and

$$\mathbf{e} = \mathbf{R}\left((2\dot{\tau} + \tau[\boldsymbol{\Omega}]_\times)[\mathbf{i}_z]_\times^T \boldsymbol{\Omega} - \tau[\mathbf{i}_z]_\times^T \mathbf{S}^{-1}\dot{\mathbf{S}}\boldsymbol{\Omega}\right). \quad (15)$$

The abbreviations c and s denote cos and sin, respectively.

III. Trajectory Tracking Control

The proposed controller aims to accurately follow the reference trajectory $\boldsymbol{\sigma}_{ref}$ by tracking not only the position and yaw references, but also their derivatives up to the fourth order. As shown in Section II-B, reference states are obtained from the high-order derivatives using the differential flatness property of the quadrotor dynamics. These reference states are used as feedforward control inputs in the trajectory tracking control. The resulting control design consists of several components based on various control methods, as given in Table I.

In order to apply INDI linear and angular acceleration control, the current accelerations are obtained through accelerometer measurements and differentiated gyroscope measurements [8]. The inertial measurement unit (IMU) signals are filtered using a digital second-order Butterworth low-pass filter (LPF) to alleviate the effects of airframe vibrations and other noise sources. We denote the LPF linear acceleration output (in body-fixed reference frame) $\mathbf{a}_f^b$, and the LPF angular rate output $\boldsymbol{\Omega}_f$. The derivative $\dot{\boldsymbol{\Omega}}_f$ is readily available if a canonical realization is used for integration of the LPF dynamics. We use $\mathbf{a}_f$ to denote the gravity-corrected LPF acceleration output in the inertial reference frame, *i.e.*,

$$\mathbf{a}_f = \mathbf{R}\mathbf{a}_f^b + g\mathbf{i}_z. \quad (16)$$

A. PD Position and Velocity Control

Position and velocity control is based on the following Proportional-Derivative (PD) controller:

$$\mathbf{a}_c = \mathbf{K}_\mathbf{x}(\mathbf{x}_{ref} - \mathbf{x}) + \mathbf{K}_\mathbf{v}(\mathbf{v}_{ref} - \mathbf{v}) + \mathbf{K}_\mathbf{a}(\mathbf{a}_{ref} - \mathbf{a}_f) + \mathbf{a}_{ref} \quad (17)$$

with $\mathbf{K}_\bullet$ indicating diagonal gain matrices.

Throughout this paper, we use the subscript c to indicate commanded values that are computed in one of the control loops. In contrast, the subscript ref indicates a value obtained directly from the reference trajectory, *e.g.*, $\mathbf{a}_c$ includes control terms based on the position and velocity deviations, while $\mathbf{a}_{ref}$ is obtained directly from the reference trajectory as the second derivative of $\mathbf{x}_{ref}$.

B. INDI Linear Acceleration Control

An INDI-based quadcopter linear acceleration controller was derived based on Taylor series approximation in [13]. In this section, we arrive at equivalent control equations using a derivation based on the estimation of the external forces acting on the quadrotor. We find that this derivation helps intuitive understanding of the practical working of INDI.

By rewriting (2), we obtain an expression for the external force acting on the quadrotor in terms of measured acceleration and specific thrust, as follows:

$$\mathbf{f}_{ext} = m(\mathbf{a}_f - \tau_f\mathbf{b}_z - g\mathbf{i}_z) \quad (18)$$

with τ_f the specific thrust calculated according to (5) using filtered motor speed measurements $\boldsymbol{\omega}_f$. The identical LPF is applied to both IMU measurements and measured motor speeds to ensure that the same phase lag is incurred by both signals [12].

Changes in $\mathbf{f}_{ext}$ are difficult to predict, so we treat it as a constant and substitute its expression (18) into (2):

$$\begin{aligned}\mathbf{a} &= \tau\mathbf{b}_z + g\mathbf{i}_z + m^{-1}\mathbf{f}_{ext} \\ &= \tau\mathbf{b}_z + g\mathbf{i}_z + m^{-1}(m(\mathbf{a}_f - \tau_f\mathbf{b}_z - g\mathbf{i}_z)) \\ &= \tau\mathbf{b}_z - \tau_f\mathbf{b}_z + \mathbf{a}_f.\end{aligned} \quad (19)$$

Even though $\mathbf{f}_{ext}$ is considered as a constant in (19), fast changes in external force are in practice accounted for by setting the IMU rate sufficiently high.

Based on (19), we compute the specific thrust vector command that results in the commanded acceleration as prescribed by (17), using the following incremental relation:

$$(\tau\mathbf{b}_z)_c = \tau_f\mathbf{b}_z + \mathbf{a}_c - \mathbf{a}_f. \quad (20)$$

The incremental nature of (20) eliminates the need for integral action; if the commanded acceleration is not immediately achieved, the thrust and attitude commands will be incremented further in subsequent control updates. Consequently, no integrator gains are needed in (17).

The commanded thrust can directly be obtained as

$$T_c = -m\|(\tau\mathbf{b}_z)_c\|_2 \quad (21)$$

with the negative sign following from the definition that thrust is positive in $\mathbf{b}_z$-direction, and the commanded roll

TABLE I: Overview of trajectory tracking controller components.

Component	Methodology	Reference	Control Output	Description
Position and Velocity Control	PD	$\mathbf{x}_{ref}$, $\mathbf{v}_{ref}$, $\mathbf{a}_{ref}$	$\mathbf{a}_c$	Section III-A
Linear Acceleration Control	INDI	$\mathbf{a}_c$	ϕ_c, θ_c, T_c	Section III-B
Jerk and Snap Tracking	Differential Flatness	$\mathbf{j}_{ref}$, $\mathbf{s}_{ref}$, $\dot{\psi}_{ref}$, $\ddot{\psi}_{ref}$	$\dot{\boldsymbol{\xi}}_{ref}$, $\ddot{\boldsymbol{\xi}}_{ref}$	Section II-B
Attitude and Attitude Rate Control	NDI	ϕ_c, θ_c, ψ_{ref}, $\dot{\boldsymbol{\xi}}_{ref}$, $\ddot{\boldsymbol{\xi}}_{ref}$	$\dot{\boldsymbol{\Omega}}_c$	Section III-C
Angular Acceleration Control	INDI	$\dot{\boldsymbol{\Omega}}_c$	$\boldsymbol{\mu}_c$	Section III-D
Moment and Thrust Control	Inversion	$\boldsymbol{\mu}_c$, T_c	$\boldsymbol{\omega}_c$	Section III-E
Motor Speed Control	Integrative	$\boldsymbol{\omega}_c$	$\boldsymbol{\zeta}$	Section III-E

ϕ_c and pitch θ_c are uniquely defined by the following expressions, based on trigonometric interpretation of $\mathbf{b}_z$ [1]:

$$\phi_c = \arcsin\left(\frac{(\tau\mathbf{b}_z)_c^T(\mathbf{i}_x\sin\psi_{ref} - \mathbf{i}_y\cos\psi_{ref})}{\|(\tau\mathbf{b}_z)_c\|_2}\right), \quad (22)$$

$$\theta_c = \arctan\left(\frac{(\tau\mathbf{b}_z)_c^T(\mathbf{i}_x\cos\psi_{ref} + \mathbf{i}_y\sin\psi_{ref})}{(\tau\mathbf{b}_z)_c^T\mathbf{i}_z}\right). \quad (23)$$

C. NDI Attitude and Attitude Rate Control

NDI, or feedback linearization, of the angular kinematics allows us to obtain a controller that takes into account nonlinear angular dynamics, but that can be tuned using linear techniques, such as pole placement and LQR [21]. The NDI controller is based on the dynamics system

$$\dot{\boldsymbol{\chi}} = f(\boldsymbol{\chi}) + g(\boldsymbol{\chi})\dot{\boldsymbol{\Omega}} = \underbrace{\begin{bmatrix}\mathbf{S}\boldsymbol{\Omega}\\ \mathbf{0}_{3\times1}\end{bmatrix}}_{f(\boldsymbol{\chi})} + \underbrace{\begin{bmatrix}\mathbf{0}_{3\times3}\\ \mathbf{I}\end{bmatrix}}_{g(\boldsymbol{\chi})}\dot{\boldsymbol{\Omega}} \quad (24)$$

with $\boldsymbol{\chi} = [\boldsymbol{\xi}^T\ \boldsymbol{\Omega}^T]^T$, and the output function

$$h(\boldsymbol{\chi}) = \boldsymbol{\xi}. \quad (25)$$

The body-frame angular acceleration $\dot{\boldsymbol{\Omega}}$ serves as the input of the state dynamics equation. This has two major advantages compared to using the control torque $\boldsymbol{\mu}$ as input. Firstly, the NDI controller is solely based on model-independent angular kinematics equations. Therefore it does not suffer from inversion discrepancies due to model mismatches. Secondly, the commanded body torque $\boldsymbol{\mu}$ is separately determined by the INDI controller described in Section III-D, which considers the external moment $\boldsymbol{\mu}_{ext}$ based on IMU measurements. This eliminates the need to incorporate a complicated model of the external moment in (24), and thereby further improves controller robustness and simplicity.

Feedback linearization of (24) results in the following equivalent linear double integrator system:

$$\ddot{\boldsymbol{\xi}} = \bar{\mathbf{u}}. \quad (26)$$

The virtual control $\bar{\mathbf{u}}$ is obtained using the NDI control mapping

$$\bar{\mathbf{u}} = L_f^2 h(\boldsymbol{\chi}) + L_g L_f h(\boldsymbol{\chi})\dot{\boldsymbol{\Omega}} \quad (27)$$

with $L_f^n h(\boldsymbol{\chi})$ the n-th Lie derivative of the function $h(\boldsymbol{\chi})$ with regard to the vector field f.

An attitude controller is designed to track the commanded state $\boldsymbol{\eta}_c = [\boldsymbol{\xi}_c^T\ \ \dot{\boldsymbol{\xi}}_{ref}^T]^T$. The attitude command $\boldsymbol{\xi}_c = [\phi_c\ \theta_c\ \psi_{ref}]^T$ consists of roll and pitch prescribed by the acceleration controller in (22) and (23), and yaw prescribed directly by the reference trajectory. As given by (10), the first two elements of the attitude rate command $\dot{\boldsymbol{\xi}}_{ref} = [\dot{\phi}_{ref}\ \ \dot{\theta}_{ref}\ \ \dot{\psi}_{ref}]^T$ are prescribed by the reference jerk through differential flatness, and the final element is obtained by differentiation of the reference yaw. The resulting linear controller has the form

$$\mathbf{u} = \mathbf{K}_{\boldsymbol{\xi}}(\boldsymbol{\xi}_c - \boldsymbol{\xi}) + \mathbf{K}_{\dot{\boldsymbol{\xi}}}\left(\dot{\boldsymbol{\xi}}_{ref} - \dot{\boldsymbol{\xi}}_f\right), \quad (28)$$

where $\dot{\boldsymbol{\xi}}_f$ has the subscript f because it is obtained by transformation of the filtered gyro rate $\boldsymbol{\Omega}_f$ using (3).

Through differential flatness, we also obtain the attitude acceleration reference $\ddot{\boldsymbol{\xi}}_{ref} = [\ddot{\phi}_{ref}\ \ \ddot{\theta}_{ref}\ \ \ddot{\psi}_{ref}]^T$ as a function of reference snap, and the second derivative of the reference yaw, as given by (13). This attitude acceleration reference is directly added to the virtual control $\mathbf{u}$ to obtain the commanded attitude acceleration:

$$\ddot{\boldsymbol{\xi}}_c = \mathbf{u} + \ddot{\boldsymbol{\xi}}_{ref}. \quad (29)$$

This direct addition of feedback and feedforward control inputs is permitted by linearity of (26). Finally, the commanded angular acceleration in the body-frame $\dot{\boldsymbol{\Omega}}_c$ is obtained by setting $\bar{\mathbf{u}} = \ddot{\boldsymbol{\xi}}_c$ and inverting the NDI control mapping (27), as follows:

$$\begin{aligned}\dot{\boldsymbol{\Omega}}_c &= \left(L_g L_f h(\boldsymbol{\chi})\right)^{-1}\left(\ddot{\boldsymbol{\xi}}_c - L_f^2 h(\boldsymbol{\chi})\right)\\ &= \mathbf{S}^{-1}\left(\ddot{\boldsymbol{\xi}}_c - L_f^2 h(\boldsymbol{\chi})\right). \quad (30)\end{aligned}$$

The attitude controller differs from a typical nonlinear attitude controller, because it not only tracks the attitude command, but also attitude rate and acceleration based on the trajectory jerk and snap. Essentially, the controller exploits its knowledge of the trajectory to predict future attitude commands.

D. INDI Angular Acceleration Control

Our proposed INDI controller tracks the angular acceleration command $\dot{\boldsymbol{\Omega}}_c$ obtained by (30). This command incorporates tracking of the reference snap through the feedforward term $\ddot{\boldsymbol{\xi}}_{ref}$. Trajectory tracking based on body rate control, *e.g.*, using an off-the-shelf inner-loop flight controller, is incapable of considering reference snap, because snap corresponds to the vehicle angular acceleration by (13).

State-of-the-art INDI control tracks angular acceleration based on linearization of the control effectiveness equation [12], [13]. We present an INDI implementation based on nonlinear inversion of (5), which improves the accuracy of thrust and control moment tracking, when compared to linearized inversion.

We rewrite (4) to obtain the following expression for the external moment based on the measured angular rate, angular acceleration, and control moment:

$$\boldsymbol{\mu}_{ext} = \mathbf{J}\dot{\boldsymbol{\Omega}}_f - \boldsymbol{\mu}_f + \boldsymbol{\Omega}_f \times \mathbf{J}\boldsymbol{\Omega}_f \tag{31}$$

with $\boldsymbol{\mu}_f$ the control moment in the body-fixed reference frame, obtained from the measured motor speed $\boldsymbol{\omega}_f$ by (5).

Analogous to the external force in Section III-B, the external moment $\boldsymbol{\mu}_{ext}$ is considered a constant, because its behavior is unmodeled. Substitution of (31) into (4) then gives:

$$\begin{aligned}\dot{\boldsymbol{\Omega}} &= \mathbf{J}^{-1}(\boldsymbol{\mu} + \boldsymbol{\mu}_{ext} - \boldsymbol{\Omega} \times \mathbf{J}\boldsymbol{\Omega}) \\ &= \mathbf{J}^{-1}(\boldsymbol{\mu} + (\mathbf{J}\dot{\boldsymbol{\Omega}}_f - \boldsymbol{\mu}_f + \boldsymbol{\Omega}_f \times \mathbf{J}\boldsymbol{\Omega}_f) - \boldsymbol{\Omega} \times \mathbf{J}\boldsymbol{\Omega}) \\ &= \dot{\boldsymbol{\Omega}}_f + \mathbf{J}^{-1}(\boldsymbol{\mu} - \boldsymbol{\mu}_f). \end{aligned} \tag{32}$$

The change in the contribution of angular momentum is neglected under the assumption of separation of time scales; it is assumed to be much slower changing compared to the motor dynamics. By inversion of the final line of (32), we obtain the control moment command required to achieve the commanded angular acceleration $\dot{\boldsymbol{\Omega}}_c$, as follows:

$$\boldsymbol{\mu}_c = \boldsymbol{\mu}_f + \mathbf{J}\left(\dot{\boldsymbol{\Omega}}_c - \dot{\boldsymbol{\Omega}}_f\right). \tag{33}$$

E. Inversion-Based Moment and Thrust Control, and Integrative Motor Speed Control

At this point, we have computed the commanded thrust T_c and control moment $\boldsymbol{\mu}_c$ by (21) and (33), respectively. Tracking of these commands requires control of the motor speeds as can be observed from the direct relation given in (5). Fast and accurate motor speed control can be achieved using loop closure based on motor speed feedback. Moreover, accurate motor speed measurements are also required in INDI control for calculation of τ_f and $\boldsymbol{\mu}_f$ in (20) and (33), respectively. To obtain the motor speeds, we employ an optical encoder that measures the motor rotation period by detecting the passage of a reflective strip on the side of the motor hub. The optical encoder, shown in Fig. 2, provides a high-rate, accurate, lightweight and unintrusive manner to obtain the motor speed.

The commanded thrust and control moment are used to solve (5) for the commanded motor speeds. In order to do so, the equation is discretized using finite-difference approximation over the time interval Δt, resulting in the following relation:

$$\begin{bmatrix} \boldsymbol{\mu}_c \\ T_c \end{bmatrix} = \mathbf{G}_1\boldsymbol{\omega}_c^{\circ 2} + \Delta t^{-1}\mathbf{G}_2(\boldsymbol{\omega}_c - \boldsymbol{\omega}_f), \tag{34}$$

which can be solved numerically, *e.g.*, using Newton's method, to obtain the commanded motor speed vector $\boldsymbol{\omega}_c$. Inversion of this nonlinear control effectiveness relation improves the accuracy of thrust and control moment tracking, when compared to linearized inversion, *e.g.*, as shown in [13].

Fig. 2: Motor (propeller removed) with optical encoder that measures rotation speed. The optical encoder lens, and accompanying reflective strip can be seen to the right, and on the front side of the motor hub, respectively.

TABLE II: Tracking performance for experiments with various reference trajectory parameters.

k [rad/s]	1.125	0.9	0.9	0.9
$\dot{\psi}_{ref}$ [rad/s]	0	0	$\frac{\pi}{2}$	π
RMS $\|\mathbf{x}-\mathbf{x}_{ref}\|_2$ [cm]	4.0	1.8	2.0	2.8
max $\|\mathbf{x}-\mathbf{x}_{ref}\|_2$ [cm]	9.4	4.1	4.8	6.5
RMS $\|\psi-\psi_{ref}\|$ [deg]	15	6.7	6.7	5.0
max $\|\psi-\psi_{ref}\|$ [deg]	36	14	21	16
RMS $\|\mathbf{v}\|_2$ [m/s]	4.2	3.3	3.3	3.3
max $\|\mathbf{v}\|_2$ [m/s]	8.2	6.6	6.6	6.6
RMS $\|\mathbf{a}-g\mathbf{i}_z\|_2$ [m/s^2]	13	11	11	11
max $\|\mathbf{a}-g\mathbf{i}_z\|_2$ [m/s^2]	19	15	15	15

The pulse width modulation vector $\boldsymbol{\zeta}$ contains the commands that are sent to the four ESCs, and is obtained as follows:

$$\boldsymbol{\zeta} = p(\boldsymbol{\omega}_\mathbf{c}) + \mathbf{K}_{\mathbf{I}_\omega}\int \boldsymbol{\omega}_c - \boldsymbol{\omega}\,\mathrm{d}\,t \tag{35}$$

with p a vector-valued polynomial function relating motor speeds to PWM inputs. This function was obtained by regression analysis of static test data. Integral action is added to account for loss of control effectiveness with decreasing battery voltage. The measured signal $\boldsymbol{\omega}$ remains unfiltered here to minimize phase lag.

IV. Experimental Results

In this section, experimental results for high-speed, high-acceleration flight are presented.

A. Experimental Setup

Experiments were performed in an indoor flight room using the quadcopter shown in Fig. 1. The 980 g quadcopter carries a Nvidia Jetson TX2 for control computations at 500 Hz, and an IMU to obtain linear acceleration and angular rate measurements at 100 Hz. Position, velocity, and orientation are obtained from a motion capture system at 360 Hz. Optical encoders are attached to the motors to measure the motor speeds at 400 Hz. Low-pass filtering of IMU and motor speed measurements is performed using a software second-order Butterworth filter with cutoff frequency 188.5 rad/s (30 Hz).

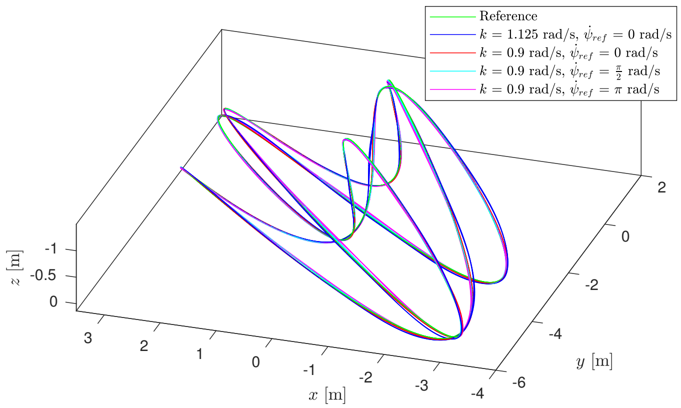

Fig. 3: Trajectories for experiments with various reference trajectory parameters.

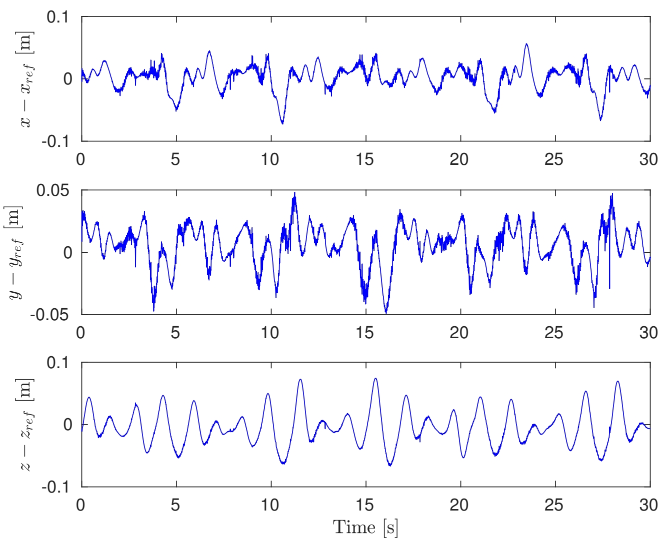

(a) Components in the inertial reference frame for $k = 1.125$ rad/s, $\dot{\psi}_{ref} = 0$ rad/s.

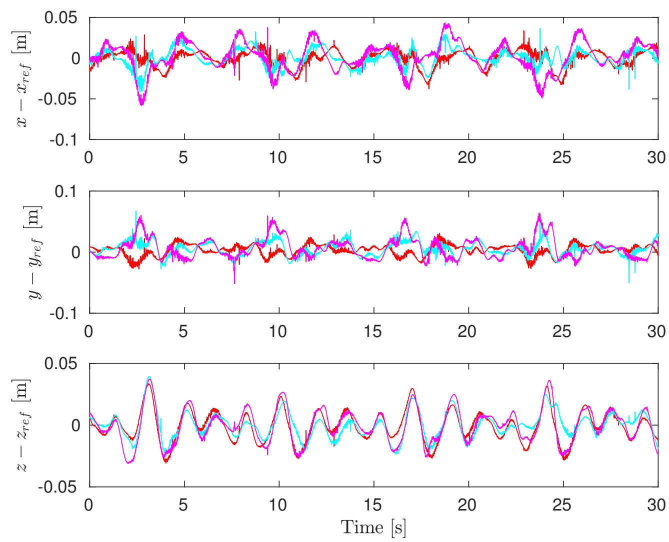

(b) Components in the inertial reference frame for $k = 0.9$ rad/s, $\dot{\psi}_{ref} = 0$ rad/s (red); $k = 0.9$ rad/s, $\dot{\psi}_{ref} = \frac{\pi}{2}$ rad/s (cyan); and $k = 0.9$ rad/s, $\dot{\psi}_{ref} = \pi$ rad/s (magenta).

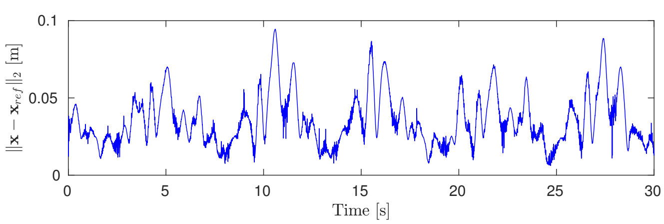

(c) Euclidean norm for $k = 1.125$ rad/s, $\dot{\psi}_{ref} = 0$ rad/s.

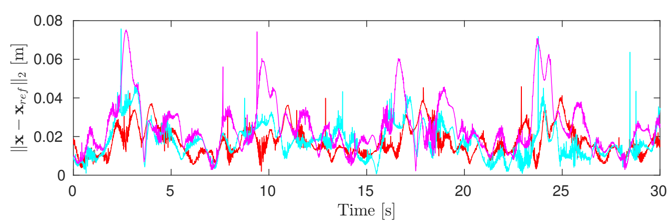

(d) Euclidean norm for $k = 0.9$ rad/s, $\dot{\psi}_{ref} = 0$ rad/s (red); $k = 0.9$ rad/s, $\dot{\psi}_{ref} = \frac{\pi}{2}$ rad/s (cyan); and $k = 0.9$ rad/s, $\dot{\psi}_{ref} = \pi$ rad/s (magenta).

Fig. 4: Position tracking error.

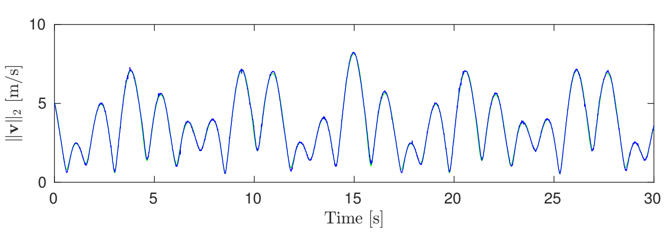

Fig. 5: Euclidean norm of velocity for reference trajectory (green) and experiment (blue) with $k = 1.125$ rad/s, $\dot{\psi}_{ref} = 0$ rad/s.

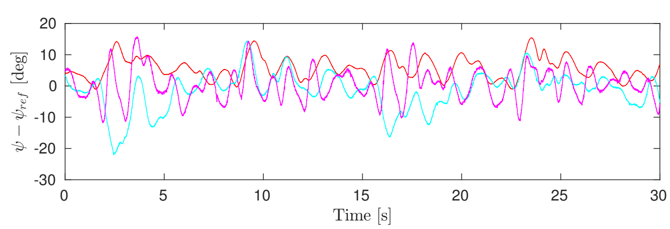

Fig. 6: Yaw error for experiments with $k = 0.9$ rad/s, $\dot{\psi}_{ref} = 0$ rad/s (red); $k = 0.9$ rad/s, $\dot{\psi}_{ref} = \frac{\pi}{2}$ rad/s (cyan); and $k = 0.9$ rad/s and $\dot{\psi}_{ref} = \pi$ rad/s (magenta).

B. Evaluation of Proposed Controller

We evaluate the performance of the trajectory tracking controller on a complicated 3D trajectory, defined as follows:

$$\boldsymbol{\sigma}_{ref}(t) = \begin{bmatrix} r_{xy}\left(\sin kt + \cos kt - \cos 2kt\right) \\ r_{xy}\left(\cos kt - \cos 2kt + \cos \frac{2}{3}kt - 1\right) \\ r_z\left(\cos 2kt + \sin kt - 1\right) \\ \dot{\psi}_{ref}t \end{bmatrix} \quad (36)$$

with $r_{xy} = 1.5$ m, $r_z = 0.5$ m, and k a parameter used to set velocity. The reference yaw rate $\dot{\psi}_{ref}$ is constant. Figure 3 shows the reference trajectory, along with experimental results for various k and $\dot{\psi}_{ref}$. Corresponding performance data are given in Table II. Each positional reference lap is traversed in $\frac{6\pi}{k}$ s, but the yaw angle reference signal is not synchronized between these laps.

The experiment with $k = 1.125$ rad/s reaches a maximum speed of 8.2 m/s, while maintaining an RMS position tracking error of 4.0 cm. The position error components and Euclidean norm are shown in respectively Fig. 4a and Fig. 4c, and the trajectory speed is shown in Fig. 5. The vehicle attains a maximum acceleration of 19 m/s^2 (2 g).

To demonstrate trajectory tracking performance in flight with high commanded yaw rate, three flights are performed with $k = 0.9$ rad/s, and $\dot{\psi}_{ref} = 0$ rad/s, $\dot{\psi}_{ref} = \frac{\pi}{2}$ rad/s and $\dot{\psi}_{ref} = \pi$ rad/s, respectively. The resulting position error is shown in Fig. 4b and Fig. 4d. It can be seen that the trajectory tracking controller is able to maintain accurate tracking of the position reference, even if a high yaw rate is prescribed. An RMS position tracking error of no more than 2.0 cm is achieved for $\dot{\psi}_{ref} = 0$ rad/s and $\dot{\psi}_{ref} = \frac{\pi}{2}$ rad/s. For $\dot{\psi}_{ref} = \pi$ rad/s, the error increases somewhat to 2.8 cm. Figure 6 shows that yaw tracking performance is consistent even for large yaw rates.

V. Conclusions

In this paper, we studied the problem of designing control systems for the tracking of aggressive, *i.e.*, fast and agile, trajectories for quadrotor vehicles. We proposed a novel control system based on incremental nonlinear dynamic inversion and differential flatness to track position and yaw angle with their derivatives of up to fourth order, specifically, the position, velocity, acceleration, jerk, and snap along with the yaw angle, yaw rate and yaw acceleration. The tracking of reference snap is enabled by closed-loop control of the propeller speeds using optical encoders attached to each motor hub. The robust control design eliminates the need for modeling or estimation of aerodynamic drag parameters. The controller achieves 4.0 cm RMS position tracking error in agile and fast flight, reaching a top speed of 8.2 m/s and acceleration of 2g, in a 6.5 m long, 6.5 m wide, and 1.5 m tall flight volume.

Acknowledgment

The authors thank Jasper Arneberg, Thomas Sayre-McCord, Varun Murali, and Winter Guerra, for help with the experiments. This work was supported in part by the Office of Naval Research (ONR) through grant N00014-17-1-2670.

References

[1] E. Tal and S. Karaman, "Accurate tracking of aggressive quadrotor trajectories using incremental nonlinear dynamic inversion and differential flatness," *arXiv preprint arXiv:1809.04048*, 2018.

[2] M. Faessler, A. Franchi, and D. Scaramuzza, "Differential flatness of quadrotor dynamics subject to rotor drag for accurate tracking of high-speed trajectories," *IEEE Robotics and Automation Letters*, vol. 3, no. 2, pp. 620–626, 2018.

[3] J. Svacha, K. Mohta, and V. Kumar, "Improving quadrotor trajectory tracking by compensating for aerodynamic effects," in *Unmanned Aircraft Systems (ICUAS), International Conference on*, pp. 860–866, IEEE, 2017.

[4] J.-M. Kai, G. Allibert, M.-D. Hua, and T. Hamel, "Nonlinear feedback control of quadrotors exploiting first-order drag effects," in *20th IFAC World Congress*, vol. 50, pp. 8189–8195, IFAC, 2017.

[5] H. Liu, D. Li, Z. Zuo, and Y. Zhong, "Robust three-loop trajectory tracking control for quadrotors with multiple uncertainties," *IEEE Transactions on Industrial Electronics*, vol. 63, no. 4, pp. 2263–2274, 2016.

[6] H. Huang, G. M. Hoffmann, S. L. Waslander, and C. J. Tomlin, "Aerodynamics and control of autonomous quadrotor helicopters in aggressive maneuvering," in *Robotics and Automation (ICRA), IEEE International Conference on*, pp. 3277–3282, IEEE, 2009.

[7] A. P. Schoellig, F. L. Mueller, and R. D'Andrea, "Optimization-based iterative learning for precise quadrocopter trajectory tracking," *Autonomous Robots*, vol. 33, no. 1-2, pp. 103–127, 2012.

[8] S. Sieberling, Q. Chu, and J. Mulder, "Robust flight control using incremental nonlinear dynamic inversion and angular acceleration prediction," *AIAA Journal of Guidance, Control, and Dynamics*, vol. 33, no. 6, pp. 1732–1742, 2010.

[9] P. Simplício, M. Pavel, E. Van Kampen, and Q. Chu, "An acceleration measurements-based approach for helicopter nonlinear flight control using incremental nonlinear dynamic inversion," *Control Engineering Practice*, vol. 21, no. 8, pp. 1065–1077, 2013.

[10] P. Smith, "A simplified approach to nonlinear dynamic inversion based flight control," in *AIAA Atmospheric Flight Mechanics Conference*, pp. 4461–4469, AIAA, 1998.

[11] B. Bacon and A. Ostroff, "Reconfigurable flight control using nonlinear dynamic inversion with a special accelerometer implementation," in *AIAA Guidance, Navigation, and Control Conference and Exhibit*, pp. 4565–4579, AIAA, 2000.

[12] E. J. Smeur, Q. P. Chu, and G. C. de Croon, "Adaptive incremental nonlinear dynamic inversion for attitude control of micro air vehicles," *AIAA Journal of Guidance, Control, and Dynamics*, vol. 38, no. 12, pp. 450–461, 2015.

[13] E. J. Smeur, G. C. de Croon, and Q. P. Chu, "Cascaded incremental nonlinear dynamic inversion control for MAV disturbance rejection," *Control Engineering Practice*, vol. 73, pp. 79–90, 2018.

[14] M. Fliess, J. Lévine, P. Martin, and P. Rouchon, "Sur les systèmes non linéaires différentiellement plats," *CR Acad. Sci. Paris*, pp. 619–624, 1992.

[15] T. Koo and S. Sastry, "Output tracking control design of a helicopter model based on approximate linearization," in *Decision and Control (CDC), 37th IEEE Conference on*, pp. 3635–3640, IEEE, 1998.

[16] P. Martin, "Aircraft control using flatness," in *Control, Optimization and Supervision, IMACS/IEEE-SMC Multiconference and CESA Symposium on*, pp. 194–199, IEEE, 1996.

[17] G. Rivera and O. Sawodny, "Flatness-based tracking control and nonlinear observer for a micro aerial quadcopter," in *Numerical Analysis and Applied Mathematics (ICNAAM), International Conference on*, pp. 386–389, American Institute of Physics, 2010.

[18] J. Ferrin, R. Leishman, R. Beard, and T. McLain, "Differential flatness based control of a rotorcraft for aggressive maneuvers," in *Intelligent Robots and Systems (IROS), IEEE/RSJ International Conference on*, pp. 2688–2693, IEEE, 2011.

[19] T. Engelhardt, T. Konrad, B. Schäfer, and D. Abel, "Flatness-based control for a quadrotor camera helicopter using model predictive control trajectory generation," in *Control and Automation (MED), 24th Mediterranean Conference on*, pp. 852–859, IEEE, 2016.

[20] D. Mellinger and V. Kumar, "Minimum snap trajectory generation and control for quadrotors," in *Robotics and Automation (ICRA), IEEE International Conference on*, pp. 2520–2525, IEEE, 2011.

[21] S. Sastry, *Nonlinear systems: Analysis, stability, and control*. Springer-Verlag, New York, 1999.